Hindawi
Advances in Civil Engineering
Volume 2022, Article ID 6578331, 12 pages
https://doi.org/10.1155/2022/6578331

Review Article

Predicting Tunnel Groundwater Inflow by Geological Investigation Using Horizontal Directional Drilling Technology

Xialin Liu

CCCC Second Highway Consultants Co., Ltd., Wuhan 430056, China

Correspondence should be addressed to Xialin Liu; liuxialin@ccccltd.cn

Received 12 August 2022; Accepted 27 September 2022; Published 13 October 2022

Academic Editor: Junpeng Zou

To improve the prediction accuracy of tunnel excavation groundwater inflow, a prediction method based on a horizontal directional drilling geological survey is proposed. It relies on the monitoring and statistical analysis of groundwater inflow into a horizontal directional drilling survey borehole. Moreover, it is based on Goodman's empirical back-calculation for the surrounding rock penetration coefficient and uses the groundwater dynamics method to predict the amount of inflow into the tunnel excavation. On the basis of an analysis of the Tianshan Shengli Tunnel, the following conclusions were obtained: the tunnel excavation groundwater inflow prediction method based on a horizontal directional drilling geological survey borehole can be used to obtain the permeability coefficient value of the surrounding rock, which can be used in the groundwater dynamics method to improve the prediction accuracy; the groundwater runoff modulus method and the atmospheric precipitation infiltration method underestimate the prediction results for tunnel groundwater inflow; and the groundwater dynamics calculation results based on the horizontal survey hole prediction method are more reliable. Goodman's empirical formula was used to predict normal groundwater inflow within the 2,271 m length from the tunnel entrance: the normal groundwater inflow into the right tunnel was approximately 6,441 m^3/d, and the maximum groundwater inflow was approximately 19,323 m^3/d. When the tunnel crosses the fault zone, the groundwater inflow increases significantly. The normal groundwater inflow per unit footage is approximately 7.30 m^3/(d·m), and the portion of the tunnel that crosses the fault zone is a medium to strong water-rich section.

1. Introduction

With the launch and implementation of a series of national strategic plans such as the Sichuan–Tibet Railway and Western Development in China, the construction of tunnel projects in China has entered a new period of growth [1]. However, the high altitudes and the necessary burial depths for ultra-long tunnel construction in mountainous areas pose various difficulties, such as problems associated with sudden water surges, e.g., property losses and casualties. These difficulties in tunnel design and construction safety are mainly due to a lack of accurate information regarding the groundwater in the rock surrounding tunnels. Therefore, it is important to carry out research on the prediction of groundwater inflow in tunnels. Many domestic and foreign scholars have carried out research on the prediction of tunnel groundwater inflow using empirical calculations, analytical solutions, numerical analyses, and other methods to calculate tunnel groundwater inflow [1–3].

In the 1850s, deep pressurized water was developed and utilized, and scholars began to study cross-flow recharge. Goodman et al. [4] proposed a method to calculate the amount of groundwater inflow from the surrounding rock based on the theory of seepage wells, and later, Tani derived an analytical solution for groundwater inflow from the surrounding rock [5]. Hwang and Lu [6] gave a semi-analytical solution for predicting the amount of groundwater inflow considering the decline in groundwater caused by tunnel construction. Farhadian and Katibeh [7] developed a new empirical model using multiple regression analysis to evaluate groundwater inflow into circular tunnels. Chen [8] studied the calculation of subsurface unsteady well flow in a stratified, heterogeneous unconfined aquifer. He [9] constructed a tunnel water influx prediction model

based on the correlation coefficient method and limit learning machines as the theoretical basis. Zhou et al. [10] constructed an optimized combination prediction model of tunnel water influx based on a variety of single prediction models. Wang et al. [11] used the "round island model" and mapping principle as the theoretical basis to derive the prediction formula of tunnel water influx under the action of a permeable interlayer. Fu et al. [12] carried out a study on the prediction of tunnel surge based on angle-preserving mapping in the fault-affected area. The existing theories and measurement methods are mainly based on vertical drilling to predict groundwater inflow. But how to optimize the formula and parameter values to apply to the horizontal borehole is still in the initial stage.

At present, predicting tunnel groundwater inflow mainly uses methods involving traditional vertical borehole geological surveys and tunnel geological prospecting. However, the traditional vertical borehole survey method is difficult to implement in high-altitude areas with treacherous terrain and inconvenient traffic. Moreover, it is characterized by low survey efficiency, high comprehensive costs, and a long construction cycle, and, owing to the survey borehole layout, it is easy to "miss" details. The method of tunnel geological prospecting can only obtain geological information within 30–100 m of the front of the tunnel construction section, which is not ideal considering the tunnel's construction speed. To this end, Ma et al. [13] proposed a geological survey technology, a long-distance horizontal directional drilling tunnel, for high-altitude mountainous conditions, which can turn the "a hole in the ground" of traditional vertical borehole geological survey methods into a blind spot-free survey along the tunnel axis. This is very helpful in terms of fully and accurately revealing the groundwater inflow and geological conditions of fault zones along the proposed tunnel. On this basis, this paper proposes a tunnel excavation surge prediction method based on the horizontal directional drilling geological survey technology, which is good for use with the groundwater dynamics method in terms of providing the surrounding rock permeability coefficient values and improving the accuracy of the tunnel excavation surge prediction.

2. Common Methods for Predicting Tunnel Water Surges

2.1. Groundwater Runoff Modulus Method. First, we assume that the modulus of underground runoff is equal to the modulus of surface runoff. Then, according to the infiltration of atmospheric precipitation required to recharge the flow of falling springs or the flow of rivers that are recharged by groundwater, the surface runoff modulus of the tunnel is determined, which is the subsurface runoff modulus of the tunnel basin. Thereafter, the catchment area of the tunnel is determined, and one can approximately predict the normal amount of water in the tunnel.

$$Q = MA, \tag{1}$$

Here, Q is the amount of groundwater surge (m^3/d); M is the basin underground runoff modulus ($m^3/d{\cdot}km^2$); and A is the catchment area of the proposed tunnel (km^2).

2.2. Atmospheric Precipitation Infiltration Method. According to the average annual precipitation in the vicinity of the tunnel, the catchment area, the topography, the vegetation, the geology, and the hydrogeological conditions are utilized to select a suitable empirical precipitation infiltration coefficient value. This can be used to approximately predict the normal amount of water discharged from the tunnel. The formula for calculating the amount of water in the tunnel is as follows:

$$Q_1 = 2.74\alpha W A, \tag{2}$$

where Q_1 is the atmospheric rainfall recharge (m^3/d); α is the precipitation infiltration coefficient; W is the multiyear average precipitation (mm); and A is the catchment area (km^2).

2.3. Groundwater Dynamics Method. The groundwater dynamics method is a conventional hydrogeological calculation method based on the principle of groundwater dynamics. It utilizes the mathematical analysis of groundwater movement under a given boundary value and the initial value conditions to establish the analytical formula and to predict the amount of tunnel groundwater inflow. After the method generalizes the hydrogeological model, it is fast and practical. Scholars have studied many related tunnel surge predictions from empirical formulae, the most common being the Oshima Yoshi formula, the Sato Bangming formula, the Lokhe Toshiro formula, the Kosgakov formula, the Gilinsky formula, the Forschheimer formula, and the Chinese empirical formula [14–16]. A part of the analytical method of the calculation formula is shown in Table 1.

At present, the groundwater dynamics method is one of the most effective for predicting tunnel groundwater inflow, and the principle is simple and easy to apply. However, the application of this method requires a series of calculation parameters, and these parameters are obtained from on-site experiments, which are difficult for ultra-long tunnel projects with high altitudes and large burial depths, so we can only refer to the empirical values.

3. Prediction Method of Groundwater Inflow in a Tunnel Based on a Horizontal Survey Borehole

3.1. Horizontal Directional Drilling Geological Survey Technology. Horizontal directional drilling (HDD) is a trenchless, pipe-laying technology that uses anchored drilling equipment to drill into the ground at a small angle of incidence relative to the ground surface, which forms a pilot hole. It then resizes the pilot hole to the required size and loads the pipe (line) into the hole by back-dragging and the traction of the drilling rig [3, 17]. This technology is widely used in municipal, oil, and gas projects and other pipeline construction industries, and it has the advantages of fast construction speed, low cost, and minimal environmental disturbance as compared with other trenchless pipe-laying technologies [18, 19].

Table 1: List of formulae for the prediction and calculation of the groundwater inflow analytical method.

Method	Formula	Scope of application	Definition of the symbols
Kosgakov formula	$Q_s = (2\alpha K H_0 L/\ln R - \ln r)\alpha = (\pi/2) + H_0/R$	Tunnels through phreatic aquifers	Q_s—predicted stable-state water influx through the tunnel through the aquifer (m^3/d); K—permeability coefficient of the rock (m/d); H_0—distance from the original static-state water level to the center of the equivalent circle of the cave-body cross section (m); S—depth of groundwater level drop (m); L—tunnel through the length of the aquifer (m); R—tunnel surge radius of influence (m); r—equivalent circle radius of tunnel cross section (m); (single tunnel application to take the value of 3.5 m, double tunnel application to take the value of 7 m).
Goodman's empirical formula	$Q_0 = \mathrm{L}2\pi kH/\ln(4H/d)$	Trans-ridge and adjacent mountain tunnels through submerged water bodies	Q_0—predicted maximum surge into a tunnel through the aquifer (m^3/); L—tunnel through the length of the aquifer (m); K—permeability coefficient of the rock (m/d); H—vertical distance from the original static-state water level to the equivalent circle center in the tunnel cross section (m); d—diameter of the equivalent circle of the tunnel body cross section (m), $d = 2r$.
Oshima Yoshi formula	$Q_{\max} = (2\pi mK(H-r)L/\ln[4(H-r)/d])$	Submerged aquifers	$Q_{\max}$—predicted maximum possible water surge through the tunnel within the aquifer (m^3/d); K—permeability coefficient of the rock (m/d); H—vertical distance from the original static-state water level in the aquifer to the tunnel floor (m); L—length of the tunnel through the aquifer (m); d—equivalent circle diameter of the tunnel cross section (m), $d = 2r$; m—conversion factor, generally taken as 0.86.
Empirical formula for railway survey procedures	$q_0 = 0.0255 + 1.9224KH$ $q_s = KH(0.676 - 0.06K)$	Submerged aquifers	$q0$—maximum surge predicted for the tunnel through the aquifer (m^3/d); q_s—normal surge predicted for the tunnel through the aquifer (m^3/d); K—permeability coefficient of the rock (m/d); H—vertical distance from the original static-state water level to the bottom of the tunnel distance (m).

As shown in Figure 1, trenchless horizontal directional drilling technology permits efficient guidance, directional control, and long-distance drilling capabilities; thus, drilling can be realized along a predesigned trajectory. The diameter of the hole is determined according to the size of the test tool, and the length of the hole is determined by combining the preliminary survey results and the survey requirements. A series of interrupted coring, hydraulic fracturing, integrated logging, and in-hole TV tests can be carried out in the hole to accurately investigate and measure the lithological parameters and the distribution of the ground stress field in the surrounding rock [20]. This improves upon the detection range of traditional tunnel geological prediction technology, significantly increases the accuracy of the detection line, provides more effective and accurate geological data for

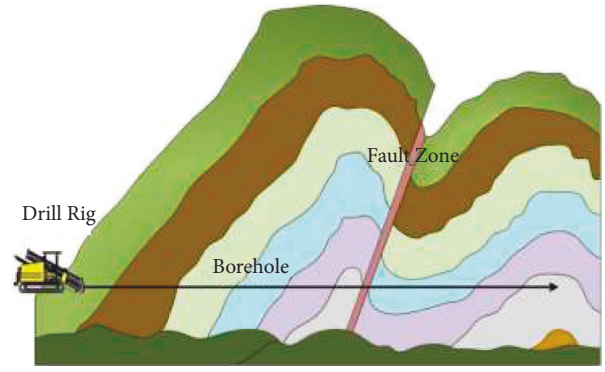

Figure 1: Schematic diagram showing horizontal directional drilling and tunneling for a geological survey.

tunnel construction, and effectively reduces the risk involved in tunnel construction.

3.2. Prediction Method of Groundwater Inflow Based on a Horizontal Survey Borehole. The borehole trajectory of the horizontal directional drilling survey is generally consistent with the centerline of the palm surface of the tunnel design trajectory. This is because the tunnel design trajectory generally has a herringbone slope, so the horizontal directional drilling survey in the tunnel entrance forms the survey hole with a certain slope. In this manner, the borehole passes through the water body exactly to provide a drainage path, and the water flow from the survey hole is natural, as shown in Figure 2.

On the basis of the horizontal directional drilling geological survey borehole, the method of predicting tunnel excavation groundwater inflow relies on the monitoring and statistical analysis of the groundwater inflow into the horizontal directional drilling survey borehole. The groundwater dynamics method is used to predict the tunnel excavation groundwater inflow. This mainly involves the following:

(1) The variation in water surges in the horizontal directional drilling survey boreholes and changes in drilling footage are monitored and recorded.

(2) The weather conditions at the tunnel site area are monitored and recorded.

(3) According to the aforementioned parameters, the changes in groundwater inflow in the horizontal directional drilling survey borehole are recorded.

(4) According to the changes in segmental groundwater inflow into the survey hole, Goodman's empirical formula is used to back-calculate the permeability coefficient of each segment, and then the groundwater dynamics method is used to predict the tunnel excavation groundwater inflow.

(5) According to the weather conditions in the tunnel site area, the changes in the tunnel excavation groundwater inflow are recorded and analyzed.

4. Case Study

4.1. Project Overview. Tianshan Shengli Tunnel is the longest highway tunnel currently under construction. It is a separated, two-way, four-lane, extra-long tunnel with a width of 11.0 m and a height of 5.0 m. The length of the left tunnel is 22,105.00 m, and the maximum depth of the tunnel is approximately 1115.03 m; the length of the right tunnel is 22,006.7 m, and the maximum depth of the tunnel is approximately 1122.024 m. The middle guide tunnel (the service tunnel) is located between the left and right tunnels, with a length of 22,054.5 m and a width and height of 7 m × 5 m.

The Tianshan Victory Tunnel crosses the Tianshan Mountain Range, which is located in a high-altitude, Alpine region with a harsh and variable climate and complex geological conditions. According to the preliminary tunnel survey data, the Boroconu–Azikuduk Fracture (Bo–A Fracture, F6), which exists approximately 1900 m from the tunnel entrance, has long-term, active characteristics, and the fracture fragmentation zone affects bedrock for a distance of approximately 300 m along the tunnel, which is a controlling geological factor in the tunnel construction process.

As shown in Figure 3, the horizontal directional drilling technique was used for the tunnel survey, i.e., from the tunnel entrance along the tunnel axis to the location of the fault zone for the geological survey. It was combined with intermittent coring, hydraulic fracturing, comprehensive logging, in-hole TV, and other tests to analyze the lithological distribution of rocks surrounding the borehole and the occurrence of joint fissures. Furthermore, these tests were used to monitor and quantify the groundwater inflow into the horizontal directional drilling survey boreholes, which was later used to predict the tunnel excavation groundwater inflow.

4.2. Drill Hole Gushing Water. The final depth of the horizontal directional drilling survey borehole for Tianshan Victory Tunnel was 2271 m, and the relationship curve of groundwater inflow in the borehole and the footage is shown in Figure 4.

From January 17 to January 21, 2020, with the continuous drilling of the borehole, the amount of groundwater inflow in the borehole exhibited an increasing trend, and the increment of groundwater inflow in the borehole was approximately 11 m^3/h during the whole process, i.e., 293 m of cumulative progress. Within the weathering zone at the tunnel inlet, the rock layer was observed to be more fractured, and the joints and fissures were relatively more developed. On 21 January, the drilling stopped, and on 22 January, the groundwater inflow in the borehole decreased to 9 m^3/h. On this day, the drilling was redirected. When the cumulative drilling reached 530 m on 26 January, the groundwater inflow in the borehole suddenly increased to 18 m^3/h at approximately 418 m. The drilling pressure was reduced to a minimum of 5 MPa at 410 m, and the drilling speed increased to 20 m/h. At this point, the surrounding rock was densely fractured, which is conducive to the collection of surface water and groundwater, thus the groundwater inflow increased significantly.

On 26 January, the drilling stopped, and the groundwater inflow gradually decreased. On 1 February, the drilling continued, and by 4 February, the drilling had reached 634 m. Here, the groundwater inflow first increased, then slowly decreased and stabilized at approximately 8 m^3/h. Similarly, when the drilling reached 1003 m, the groundwater inflow first increased, then slowly decreased and stabilized. After a cumulative drilling footage of 1003 m, the groundwater inflow continued to increase significantly, reaching a peak of approximately 35 m^3/h at about 2028 m. This was caused by a survey borehole moving through the core section of the Boa fault zone. Then, the survey borehole moved into a dense granite, and the groundwater inflow dropped to a minimum of approximately 14 m^3/h. At the

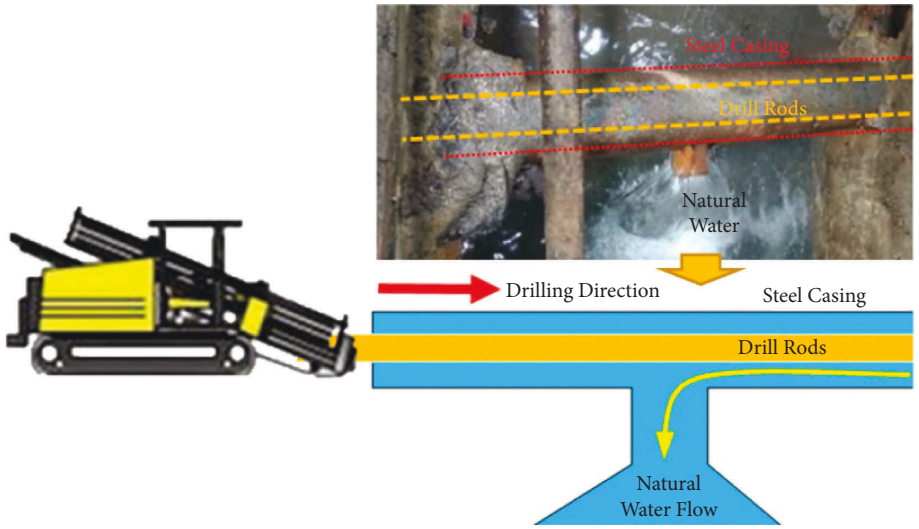

Figure 2: Natural water flowing from the survey hole (vertical view).

Figure 3: Geological survey site of the horizontal directional drilling tunnel.

end of the borehole, the survey borehole groundwater inflow suddenly increased and then decreased, perhaps due to the weather.

4.3. Parameter Values. The tunnel site is located in the tectonic denudation of a high mountain landscape area, characterized by glaciers and glacial landform development, large topographic relief, and strong rock weathering and deposition, mainly from the ice and water accumulation in debris soil.

The stratigraphy of the tunnel site area is mainly Quaternary alluvial pebbles (Q_4^{al+pl}), avalanche slope accumulation rubble (Q_4^{c+dl}), ice and water accumulation rubble (Q_4^{fgl}), Devonian upper Tianger Group gray-green tuffaceous sandstone (D_3t^b), middle Yuan Dynasty (Pt_2), Jixian System Kawabrak Group II (Jxk^2) gray-brown metamorphic sandstone, sandy slate, dacite; middle Yuan Dynasty (Pt_2) Great Wall System Xingxingxia Group (CHx) gray-green quartz schist, gneiss and Hualixian intrusive light flesh-red granite porphyry ($\gamma_C^{2d}H$) gray-white granite, granite amphibolite ($\eta\gamma_D^1H$), Garridonian intrusive gray-white granite amphibolite ($\gamma\delta_s^1Q$, $\gamma\delta_s^2Q$), and Jinning Movement intrusive gray gneissic amphibolite ($tn_{Qb}H$).

The climate of the area in which the tunnel site is located is a typical temperate continental arid climate, with a high mountain cold zone and glaciers. The surface water system is mainly composed of the Urumqi River and the Ulastai River. Groundwater is recharged mainly from atmospheric precipitation and alpine ice and snow melt.

The topographic and geomorphological conditions of the tunnel site area, the lithological characteristics of the strata, and the distribution and hydraulic head of groundwater in the aquifer were considered to determine the choice of groundwater runoff modulus method: the atmospheric precipitation infiltration method, the Kosgakov formula, the empirical railroad formula for the tunnel normal groundwater inflow prediction, the choice of Goodman's empirical formula, the Oshima Yoshi formula, and the empirical railroad formula for the tunnel maximum groundwater inflow prediction.

4.3.1. Groundwater Runoff Modulus M. According to the reports "Groundwater Resources in Xinjiang" and "Hydrogeological Survey Report of Tianshan Shengli Tunnel," the groundwater runoff modulus in the mountainous area of the Ulastai basin is 134.24 $m^3/d{\cdot}km^2$, the groundwater runoff modulus in the mountainous area of the Urumqi River is 216 $m^3/d{\cdot}km^2$, and the groundwater runoff modulus in the mountainous area of the Alagou River basin is 99.4 $m^3/d{\cdot}km^2$.

4.3.2. Atmospheric Precipitation Infiltration Coefficient a. According to the preliminary survey data, the rock layer at the Boa fault is extremely fractured, the fracture right-hand misalignment is large, there is a long-term activity, and there is abundant mud and sand fill. Using tunnel engineering experience, the empirical value for the Boa fault zone precipitation infiltration coefficient was determined at 0.40.

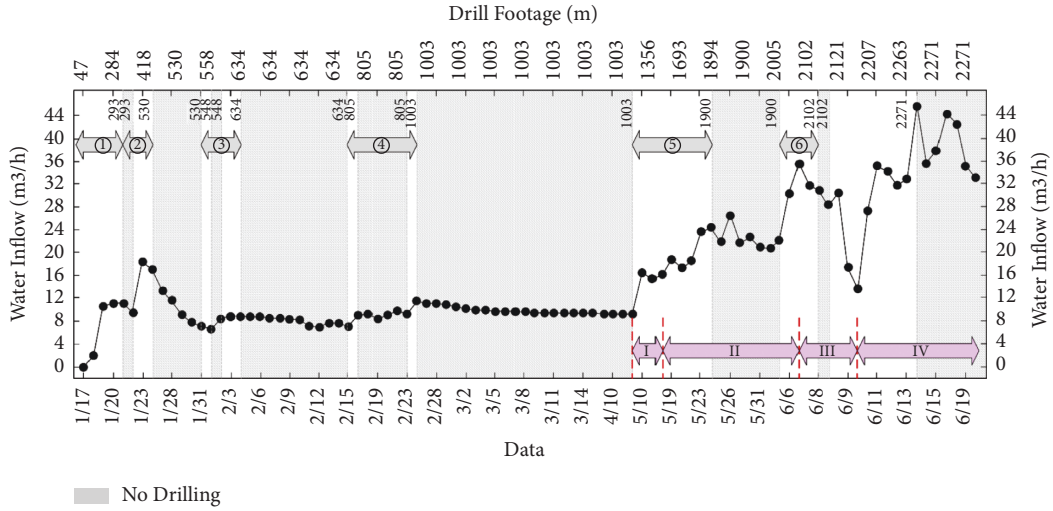

Figure 4: The relationship curve of groundwater inflow in the borehole and the footage.

Moreover, for the tunnel plan projection in the geomorphological unit, i.e., climate zoning, $a = 0.15 \sim 0.40$.

4.3.3. Water Hydraulic Head H. The vertical drilling information and the distribution of rivers in the tunnel site area were combined to determine the groundwater level, and H was used to establish the average difference in hydraulic head between the borehole level and the groundwater level.

4.3.4. Permeability Coefficient K. From the previous hydrogeological tests and horizontal directional drilling survey borehole, the site data were used to establish the value of the permeability coefficient K. When no site survey data are available, the *Hydrogeology Manual (Second Edition)* [20] and similar projects on the permeability coefficient K can be used to establish the empirical value. As shown in Figure 4, considering the above analysis of the groundwater inflow into the horizontal directional drilling borehole, the drilling footage was divided into seven sections using Goodman's empirical back-calculation of the permeability coefficient value for each section. The calculation results are shown in Table 2.

Because the seventh section of the survey hole groundwater inflow was affected to a large extent by weather factors, the permeability coefficient K value was established with reference to the vertical hole prehydrogeological test results. The permeability coefficient values of different lithological sections are shown in Table 3. In the fracture fragmentation zone and its influence zone, the permeability coefficient of the stratum increases significantly. Owing to a lack of relevant data on the permeability performance of the fault zone in the evaluation area, empirical values were adopted for the permeability coefficients in this area. In addition, the permeability coefficient values for the fault zone and its influence zone decrease with an increase in burial depth. The permeability coefficient values for the Boa fault and other fractures at different burial depths are shown in Table 4. These are based on the results of existing hydrogeological tests and the characteristics of the permeability performance of the fault zones.

According to the vertical distribution characteristics of the permeability properties of the fault zone, the fault zone is regarded as composed of laminated strata with different permeabilities in the vertical direction. Thus, the equivalent permeability coefficient K of the fault zone when the groundwater flows perpendicular to the direction of the level under the tunnel burial depth condition was calculated using the following equation:

$$K = \frac{\sum_{i=1}^{n} M_i}{\sum_{i=1}^{n} M_i / K_i}, \tag{3}$$

where M_i and K_i are the thickness (m) and permeability coefficient value (m/d), respectively, of the ith stratum.

4.3.5. The Depth of the Groundwater Level Drop S. Previously, when calculating the tunnel surge, for the import section and export section of the weathered zone and through the gully zone, the difference in the hydraulic head S was often taken as the distance from the groundwater level to the tunnel floor. For the deep-buried belt, the formula proposed by Wan [21] was used to calculate the reduction in S with depth:

$$S = \left(1 - e^{-0.72K}\right)H, \tag{4}$$

where K is the permeability coefficient (m/d) and H is the water head height (m).

4.3.6. Radius of the Area of Influence R. For the weathered zone and the valley-crossing zone, the radius of influence R was delineated according to the topography. For the bedrock section, it was determined according to the formula recommended by the Regulations for Hydrogeological Investigation of Railway Engineering (TB 10049-2014) [14]:

Table 2: Permeability coefficient of each section of the horizontal directional drilling exploration borehole, based on Goodman's empirical back-calculation.

Serial of drilling segments	Range of depth (m)	Construction	Increment of groundwater inflow Q (m^3/h)	Height of hydraulic head H (m)	Diameter of the drilled hole d (m)	Length of water-bearing Body L (m)	Permeability coefficient K (m/d)
①	0–293	Weathered zone	11	17.5	0.25	263	0.0514
②	293–530	Through the gully zone	9	50	0.25	125	0.0368
③	530–634	Deep buried zone	2	150	0.25	112	0.0035
④	634–1003	Deep buried zone	4.29	300	0.25	369	0.00125
⑤	1003–1900	Deep buried zone	17.19	400	0.25	897	0.0016
⑥	1900–2102	Deep buried zone	13.41	400	0.25	128	0.0088

Table 3: Table of hydrogeological test results.

Serial	Number of drilled holes	Stakes of the mileage	Lithology of the strata	Permeability coefficient (m/d)
1	SZK01	ZK75 + 866 right 15.6 m	Tuffaceous sandstone	8.406×10^{-4}
2	SZK02	YK79 + 361 right 272.7 m	Medium-weathered granite, quartz schist	2.714×10^{-3}
3	SZK03	YK81 + 356 right 195 m	Quartz schist	2.819×10^{-3}
4	SZK04	ZK84 + 140 left 40 m	Granite	9.89×10^{-4}
5	SZK05	ZK87 + 248.7 left 40 m	Granite	9.26×10^{-4}
6	SZK06	YK93 + 300 right 120 m	Quartz schist	5.471×10^{-3}
7	SZK07	ZK93 + 493.5 left 100.5 m	Quartz schist	4.321×10^{-3}

Table 4: Permeability coefficient values of the tunnel passing through the fault zone and the surrounding rock in the affected zone.

Tunnel depth (m)	<80 m	80~150 m	150~250 m	250~350 m	>350 m
Permeability coefficient of Bo–A fault zone (m/d)	0.5 (experience value)	0.2	0.05	0.01	0.005
Permeability coefficients of other fault zones (m/d)	0.1 (experience value)	0.05	0.01	0.005	0.002

$$\begin{aligned} R &= 215.5 + 510.5K, \\ B &= 2R, \end{aligned} \tag{5}$$

where R denotes the groundwater inflow on the side of the tunnel affecting the width (m); K denotes the permeability coefficient of aquifers (m/d); and B denotes the inflow of water on both sides of the tunnel affecting the width (m).

For the fault zone, the Kusakin formula was used to calculate the parameters related to the radius of influence R, including the aquifer thickness H and the permeability coefficient K:

$$R = 2H\sqrt{HK}. \tag{6}$$

4.4. Analysis of Results

4.4.1. Groundwater Runoff Modulus Method. The distance from the tunnel's entrance totaled 2271 m. On the basis of the groundwater runoff modulus method for the right tunnel, the predicted groundwater inflows are shown in Table 5. The total groundwater inflow of the right tunnel based on the groundwater runoff modulus method was 618.7 m^3/d. The average groundwater inflow into the tunnel per unit footage was 0.3575 m^3/(d·m), the minimum value was 0.0933 m^3/(d·m), the maximum value was 1.7643 m^3/(d·m), and the maximum amount of groundwater inflow per unit footage is located in the Bo–A fault zone (F6).

4.4.2. Atmospheric Precipitation Infiltration Method. The distance from the tunnel's entrance totaled 2271 m. On the basis of the atmospheric precipitation infiltration method for the right tunnel, the predicted water surge values are shown in Table 6. The total groundwater inflow into the right tunnel based on the atmospheric precipitation infiltration method was 1480.35 m^3/d. The average groundwater inflow into the tunnel per unit footage was 0.9094 m^3/(d·m), the minimum value was 0.098 m^3/(d·m), the maximum value was 5.147 m^3/(d·m), and the maximum amount of groundwater inflow per unit footage is located in the Bo–A fault zone (F6).

4.4.3. Groundwater Dynamics Method. The distance from the tunnel's entrance totaled 2271 m. On the basis of the groundwater dynamics method for the right tunnel, the predicted water surge values are shown in Table 7. Taking the right tunnel as an example, the normal groundwater inflow obtained by Goodman's empirical formula, the Kosgakov formula, the empirical railway formula, and the Oshima Yoshi's formula were 6441, 7593, 3313, and 4937 m^3/d, respectively.

Table 5: Prediction of groundwater inflow into the right tunnel based on the groundwater runoff modulus method.

Serial	Segmented mileage		Length (m)	Groundwater runoff modulus $m^3/(d{\cdot}km^2)$	Radius of influence R	Catchment area A (km^2)	Groundwater inflow Q_s (m^3/d)	Groundwater inflow perunit footage q_s $m^3/(d{\cdot}m)$
1	YK75 + 815	YK75 + 948	133.0	216.0	215.9	0.057	12.4	0.093
2	YK75 + 948	YK76 + 015	67.0	216.0	241.7	0.032	7.0	0.104
3	YK76 + 015	YK76 + 063	48.0	216.0	241.7	0.023	5.0	0.104
4	YK76 + 063	YK76 + 168	105.0	216.0	217.3	0.046	9.9	0.094
5	YK76 + 168	YK76 + 265	97.0	216.0	1471.31	0.285	61.7	0.636
6	YK76 + 265	YK76 + 580	315.0	216.0	266.20	0.168	36.2	0.115
7	YK76 + 580	YK76 + 660	80.0	216.0	1297.57	0.208	44.8	0.561
8	YK76 + 660	YK77 + 273	613.0	216.0	216.1	0.265	57.2	0.093
9	YK77 + 273	YK77 + 408	135.0	216.0	2558.09	0.691	149.2	1.105
10	YK77 + 408	YK77 + 565	157.0	216.0	216.9	0.068	14.7	0.094
11	YK77 + 565	YK77 + 591	26.0	216.0	218.3	0.011	2.5	0.094
12	YK77 + 591	YK77 + 743	152.0	216.0	218.3	0.066	14.3	0.094
13	YK77 + 743	YK77 + 839	96.0	216.0	3838.17	0.737	159.2	1.658
14	YK77 + 839	YK77 + 904	65.0	216.0	216.9	0.028	6.1	0.094
15	YK77 + 904	YK77 + 994	90.0	216.0	216.9	0.039	8.4	0.094
16	YK77 + 994	YK78 + 019	25.0	216.0	2199.56	0.110	23.8	0.950
17	YK78 + 019	YK78 + 086	67.0	216.0	216.9	0.065	6.3	0.094

Table 6: Prediction of groundwater inflow into the right tunnel based on the atmospheric precipitation infiltration method.

Serial	Segmented mileage		Length (m)	Infiltration coefficient α	Annual average rainfall (mm)	Radius of influence R (m)	Catchment area A (km^2)	Groundwater inflow Q_s (m^3/d)	Groundwaterinflow perunit footage q_s $m^3/(d{\cdot}m)$
1	YK75 + 815	YK75 + 948	133.0	0.25	550.0	241.7	0.064	24.23	0.182
2	YK75 + 948	YK76 + 015	67.0	0.25	550.0	241.7	0.032	12.20	0.182
3	YK76 + 015	YK76 + 063	48.0	0.25	550.0	241.7	0.023	8.74	0.182
4	YK76 + 063	YK76 + 168	105.0	0.25	550.0	217.3	0.046	17.19	0.164
5	YK76 + 168	YK76 + 265	97.0	0.4	550.0	1471.31	0.285	172.06	1.774
6	YK76 + 265	YK76 + 580	315.0	0.2	550.0	216.1	0.136	41.04	0.130
7	YK76 + 580	YK76 + 660	80.0	0.4	550.0	1297.57	0.208	125.15	1.564
8	YK76 + 660	YK77 + 273	613.0	0.2	550.0	216.1	0.265	79.87	0.130
9	YK77 + 273	YK77 + 408	135.0	0.4	550.0	2558.09	0.691	416.34	3.084
10	YK77 + 408	YK77 + 565	157.0	0.2	550.0	216.9	0.068	20.53	0.131
11	YK77 + 565	YK77 + 591	26.0	0.2	550.0	218.3	0.011	3.42	0.132
12	YK77 + 591	YK77 + 743	152.0	0.2	550.0	218.3	0.066	20.00	0.132
13	YK77 + 743	YK77 + 839	96.0	0.4	550.0	3838.17	0.737	444.22	4.627
14	YK77 + 839	YK77 + 904	65.0	0.2	550.0	216.9	0.028	8.50	0.131
15	YK77 + 904	YK77 + 994	90.0	0.2	550.0	216.9	0.039	11.77	0.131
16	YK77 + 994	YK78 + 019	25.0	0.4	550.0	2199.56	0.110	66.29	2.652
17	YK78 + 019	YK78 + 086	67.0	0.2	550.0	216.9	0.065	8.8	0.131

By comparing the calculation results of the groundwater runoff modulus method, the atmospheric precipitation infiltration method, and the groundwater dynamics method, it can be seen that the inflow values obtained by the groundwater runoff modulus method and the atmospheric precipitation infiltration method were underestimated. This is because the groundwater runoff modulus method and the atmospheric precipitation infiltration method are essentially water equilibrium methods, and it is difficult to obtain accurate data for various parameters. Moreover, the two methods do not consider the impact of steady-state groundwater reserves on tunnel groundwater inflow, nor can they adequately characterize the impact of fault zones. Therefore, the calculation results of groundwater dynamics based on the horizontal survey hole prediction method were more reliable. In the groundwater dynamics method, the results between the various calculation formulae were also quite different, with the comprehensive comparison indicating that the normal groundwater inflow obtained by Goodman's empirical formula is superior, as the maximum groundwater inflow was three times the normal inflow.

The changes in groundwater inflow during the horizontal directional drilling of the survey borehole into the Boa

Table 7: Prediction of normal groundwater inflow into the right tunnel based on the groundwater dynamics method.

Seria	Segmented mileage		Length (m)	Permeability coefficient K (m/d)	Goodman's empirical (q_s, m^3/d·m)	Kosgakov (q_s, m^3/d·m)	Railway empirical (q_s, m^3/d·m)	Oshima Yoshi (q_s, m^3/d·m)	Goodman's empirical (Q_s, m^3/d)	Kosgakov (Q_s, m^3/d)	Railway empirical (Q_s, m^3/d)	Oshima Yoshi (Q_s, m^3/d)
1	YK75 + 815	YK75 + 948	133.0	0.0514	3.73	1.32	0.93	2.28	495.5	175.4	124.2	303.4
2	YK75 + 948	YK76 + 015	67.0	0.0514	6.45	3.41	2.21	4.55	432.3	228.4	148.3	304.5
3	YK76 + 015	YK76 + 063	48.0	0.0514	7.61	4.48	2.80	5.49	365.1	215.1	134.5	263.5
4	YK76 + 063	YK76 + 168	105.0	0.0035	0.61	0.42	0.24	0.45	64.2	44.5	25.3	47.2
5	YK76 + 168	YK76 + 265	97.0	0.0368	12.46	5.86	6.07	9.63	1208.8	568.2	589.3	934.3
6	YK76 + 265	YK76 + 580	315.0	0.00125	0.42	0.47	0.20	0.32	132.1	149.5	64.4	102.0
7	YK76 + 580	YK76 + 660	80.0	0.0088	4.06	2.26	2.16	3.18	325.1	181.1	172.6	254.7
8	YK76 + 660	YK77 + 273	613.0	0.00125	0.58	0.87	0.31	0.45	355.4	531.6	189.0	278.5
9	YK77 + 273	YK77 + 408	135.0	0.00645	4.67	2.52	2.76	3.71	630.2	339.7	372.4	500.8
10	YK77 + 408	YK77 + 565	157.0	0.002714	2.03	4.78	1.21	1.61	318.0	750.1	189.2	252.9
11	YK77 + 565	YK77 + 591	26.0	0.005471	4.97	14.30	3.08	3.97	129.2	371.9	80.2	103.2
12	YK77 + 591	YK77 + 743	152.0	0.005471	4.67	12.60	2.86	3.73	710.0	1914.7	434.9	566.5
13	YK77 + 743	YK77 + 839	96.0	0.0088	7.30	3.69	4.45	5.82	701.3	353.8	426.8	559.1
14	YK77 + 839	YK77 + 904	65.0	0.002819	2.41	6.56	1.48	1.92	156.8	426.3	96.1	125.1
15	YK77 + 904	YK77 + 994	90.0	0.002819	2.28	5.82	1.38	1.81	204.8	523.9	124.0	163.2
16	YK77 + 994	YK78 + 019	25.0	0.00365	2.84	1.66	1.71	2.26	71.1	41.4	42.7	56.6
17	YK78 + 019	YK78 + 169	150.0	0.002714	2.11	5.18	1.27	1.68	141.4	777.6	98.8	121.7

Table 8: Suggested values of normal groundwater inflow for the right tunnel.

Serial	Segmented mileage		Length L (m)	Characteristics of rock mass in the tunnel segment		Normal groundwater inflow		Water-richness zoning
	Beginning	Terminal		Stratum	Tectonics	Q_s m^3/(d·m)	Q_s (m^3/d)	
1	YK75 + 815	YK75 + 948	133.0	Tuffaceous siltstone	Weatherstripping	3.73	495.54	Medium water-rich section
2	YK75 + 948	YK76 + 015	67.0	Tuffaceous siltstone	Weatherstripping	6.45	432.31	Strong water-rich section
3	YK76 + 015	YK76 + 063	48.0	Tuffaceous siltstone	Weatherstripping	7.61	365.13	Strong water-rich section
4	YK76 + 063	YK76 + 168	105.0	Tuffaceous siltstone	—	0.61	64.19	Weakly water-rich section
5	YK76 + 168	YK76 + 265	97.0	Tuffaceous siltstone	Fw-5 fault zone/gully crossing zone	12.46	1208.82	Strong water-rich section
6	YK76 + 265	YK76 + 580	315.0	Tuffaceous siltstone	—	0.42	132.07	Weakly water-rich section
7	YK76 + 580	YK76 + 660	80.0	Tuffaceous siltstone	Fw-6 fault zone	4.06	325.11	Medium water-rich section
8	YK76 + 660	YK77 + 273	613.0	Tuffaceous siltstone	—	0.58	355.41	Weakly water-rich section
9	YK77 + 273	YK77 + 408	135.0	Tuffaceous siltstone	Fw-7 fault zone	4.67	630.25	Medium water-rich section
10	YK77 + 408	YK77 + 565	157.0	Granite diorite	—	2.03	317.95	Medium water-rich section
11	YK77 + 565	YK77 + 591	26.0	Variable sandstone plywood marble	—	4.97	129.17	Medium water-rich section
12	YK77 + 591	YK77 + 743	152.0	Granite diorite	—	4.67	710.00	Medium water-rich section
13	YK77 + 743	YK77 + 839	96.0	Granite diorite	F6 Boa fault zone	7.30	701.25	Strong water-rich section
14	YK77 + 839	YK77 + 904	65.0	Quartz schist	—	2.41	156.78	Medium water-rich section
15	YK77 + 904	YK77 + 994	90.0	Granite diorite	—	2.28	204.79	Medium water-rich section
16	YK77 + 994	YK78 + 019	25.0	Granite diorite	Fw-8 fault zone	2.84	71.05	Medium water-rich section
17	YK78 + 019	YK78 + 086	67.0	Granite diorite	—	2.11	141.37	Medium water-rich section

fault are shown in Figure 4. It can be seen from the following figure:

(1) When drilling close to the Boa fault zone, the groundwater inflow during drilling began to increase significantly from 1003 m to 1616 m (area I); the groundwater inflow increased by 6 m^3/h, and for every 100 m drilled, the groundwater inflow increased by approximately 1 m^3/h.

(2) After crossing the Boa fault, the groundwater inflow increased significantly from 1616 m to 2020 m (area II); the groundwater inflow increased by approximately 20 m^3/h, and for every 100 m drilled, the groundwater inflow increased by approximately 5 m^3/h.

(3) The source of groundwater inflow in the Boa fault zone is mainly steady-state groundwater reserves, and the recharge is not smooth, which was observed when the horizontal drilling reached 2159 m (area III). In addition, the groundwater inflow in the whole section was reduced to 14 m^3/h.

(4) After 2159 m (area IV), as a result of the frequent rainfall and snowfall and the temperature rise, a significant increase in the flow of water in the ditch was observed in the shallow burial section of the tunnel inlet section at 500 m. In addition, the water in the ditch replenishes groundwater, causing a significant increase in the amount of groundwater inflow from the horizontal directional drilling borehole survey.

For the distance within 2271 m from the entrance of the tunnel, the predicted value of the normal groundwater inflow into the right tunnel and the water-rich partition are shown in Table 8. The normal groundwater inflow into the right tunnel was approximately 6441 m^3/d, and the maximum groundwater inflow was approximately 19,323 m^3/d. When the tunnel crossed the fault zone, the groundwater inflow increased significantly, where the normal groundwater inflow per unit footage along the F6 Boa fault zone was approximately 7.30 m^3/(d·m). The section in which the tunnel crosses the fault zone is a medium to strong water-rich section, so during the tunnel construction process, it is necessary to do advanced geological forecasting, advanced pregrouting, water blockage prevention, and water inrush prevention. In addition, the tunnel crosses the glacier and permafrost zones. In the spring, as the temperature rises, the melting of snow and ice will lead to an increase in tunnel groundwater inflow, which needs to be prevented.

5. Conclusions

With the application and development of horizontal directional drilling technology for ultra-long-distance tunnels in mountainous areas at high altitudes and with large burial depths, it is necessary to improve the accuracy in predicting the surge of groundwater into the tunnel excavation. Therefore, in this paper, we propose a method for predicting the groundwater inflow into tunnels based on horizontal exploration boreholes. On the basis of a geological survey of a horizontal directional drilling borehole, we carried out research predicting groundwater inflow into a tunnel excavation. Using an analysis of the Tianshan Victory Tunnel Project as our foundation, our main conclusions are as follows:

(1) The method for predicting the amount of groundwater inflow in tunnel excavation based on horizontal directional drilling boreholes can provide the permeability coefficient value of the surrounding rock, which can be used in the groundwater dynamics method and can improve the prediction accuracy. Additionally, it is still suggested to use redesigned packers to obtain more accurate groundwater inflow data for a controlled horizontal borehole, which is more practical for engineering design and construction.

(2) The prediction results of the groundwater runoff modulus method and atmospheric precipitation infiltration method regarding the overall amount of groundwater inflow in tunnels are low, and the calculation results of groundwater dynamics based on the horizontal survey hole prediction method are more reliable.

(3) Using Goodman's empirical formula to predict normal groundwater inflow along the 2271 m distance from the tunnel entrance, the normal groundwater inflow into the right tunnel was approximately 6441 m^3/d, and the maximum groundwater inflow was approximately 19,323 m^3/d.

(4) When the tunnel crosses the fault zone, the groundwater inflow increased significantly, as the normal groundwater inflow per unit of the F6 Boa fault zone is approximately 7.30 m^3/(d·m). The zone in which the tunnel crosses the fault is a medium-to-strong water-rich section;

(5) During the tunnel construction process, it is necessary to do advanced geological forecasting, advanced pregrouting, water blockage prevention, and water inrush prevention near the fault zones. In addition, the tunnel crosses the glacier and permafrost zone. In the spring, as the temperature rises, melting snow and ice will lead to an increase in tunnel groundwater inflow, which needs to be prevented.

Data Availability

Data are available within the article.

Disclosure

The funders had no role in the design of the study; in the collection, analyses, or interpretation of data; in the writing of the manuscript, or in the decision to publish the results.

Conflicts of Interest

The author declares that there are no conflict of interest.

Authors' Contributions

Methodology, formal analysis, investigation, data curation, original draft preparation, review and editing were done by Xialin Liu. The author has read and agreed to the published version of the manuscript.

Acknowledgments

This research was supported by the Xinjiang Uygur Autonomous Region Science and Technology Major Project (No. 2020A03003-1) and the National Natural Science Foundation of China (No. 42002284).

References

[1] S. M. Tian, W. Wang, and J. F. Gong, "Development and prospect of railway tunnels in China (including statistics of railway tunnels in China by the end of 2020)," *Tunn. Constr.*vol. 41, pp. 308–325, 2021.

[2] J. Zou, Y.-Y. Jiao, F. Tan, J. Lv, and Q. Zhang, "Complex hydraulic-fracture-network propagation in a naturally fractured reservoir," *Computers and Geotechnics*, vol. 135, Article ID 104165, 2021.

[3] Y.-Y. Jiao, K. Wu, J. Zou et al., "On the strong earthquakes induced by deep coal mining under thick strata-a case study," *Geomechanics and Geophysics for Geo-Energy and Geo-Resources*, vol. 7, no. 4, 2021.

[4] R. E. Goodman, D. G. Moye, A. V. Schalkwyk, and I. Javandel, "Ground groundwater inflow during tunnel driving," *Engineering Geology*, vol. 2, pp. 39–56, 1965.

[5] M. E. Tani, "Circular tunnel in a semi-infinite aquifer. Tunnelling & underground space technology incorporating trenchless," *Technology Research*, vol. 18, pp. 49–55, 2003.

[6] J. H. Hwang and C. C. Lu, "A semi-analytical method for analyzing the tunnel water inflow," *Tunnelling and Underground Space Technology*, vol. 22, no. 1, pp. 39–46, 2007.

[7] H. Farhadian and H. Katibeh, "New empirical model to evaluate groundwater flow into circular tunnel using multiple regression analysis," *International Journal of Mining Science and Technology*, vol. 3, pp. 32–38, 2017.

[8] C. X. Chen, "Calculation method of unstable underground well flow in layered heterogeneous pressureless aquifer," *Earth Sci. -J. Wuhan Inst. Geol.*vol. 1P, 1981.

[9] H. G. He, "Prediction of groundwater inflow in karst tunnels based on correlation criterion and R-ELM model," *Tunnel Construction*, vol. 39, pp. 1262–1269, 2019.

[10] L. Zhou, G. Q. Yang, and Q. C. Yang, "Prediction of groundwater inflow in karst tunnels based on optimal combination model and rescaled range method," *Eng. J. Wuhan Univ.*vol. 53, pp. 875–882, 2020.

[11] L. F. Wang, N. Tang, and Y. Mo, "Prediction of groundwater inflow of water-rich mountain tunnel with permeable interlayer," *Science Technology and Engineering*, vol. 20, pp. 13865–13871, 2020.

[12] H. L. Fu, Z. Li, and G. W. Cheng, "Prediction of tunnel groundwater inflow in fault affected area based on conformal mapping," *Journal of Huazhong University of Science and Technology*, vol. 49, pp. 86–92, 2021.

[13] B. S. Ma, Y. Cheng, J. G. Liu, Z. Donglin, Y. Xuefeng, and Z. Qiang, "Tunnel accurate geological investigation using long distance horizontal directional drilling technology," *Tunn. Constr.*vol. 41, pp. 972–978, 2021.

[14] *TB 10049-2014; Regulations for Hydrogeological Investigation of Railway Engineering,* China Railway Publishing House Co., Ltd., China.

[15] R. Goodman, D. Moye, A. Schalkwyk, and I. Javendel, *Groundwater Inflow during Tunnel Driving*, College of Engineering, University of California, Berkeley, California, 1964.

[16] G. Q. Wang, "Research on evaluation and control of karst water Resources in a certain tunnel of dalian subway," *IOP Conference Series: Earth and Environmental Science*, vol. 153, no. 6, IOP Publishing, 2018.

[17] B. S. Ma, *Trenchless Engineering*, People's Communications Press, Beijing, China, 2008.

[18] C. Zeng and B. S. Ma, *Horizontal Directional Drilling Theory and Technology*, China University of Geosciences Press, Wuhan, China, 2015.

[19] B. S. Ma, X. F. Yan, and C. Zeng, *A Horizontal Directional Drilling Engineering Geological Survey Method. CN201910768217.X.*

[20] *China Geological Survey. Handbook of Hydrogeology*, Geological Publishing House, Beijing, China, 2012.

[21] Y. Wan, "Experimental Study on Water Bursting Model of Tunnel in Medium-Low Permeability Medium," Master's thesis, Chengdu University of Technology, Chengdu, China, 2017.